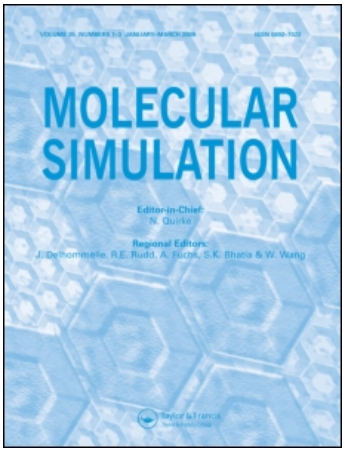

Molecular Simulation
Publication details, including instructions for authors and subscription information:
http://www.informaworld.com/smpp/title~content=t713644482

Adsorption in micropores (nanopores): a computer appraisal of the Dubinin equations

D. D. Do[a]; D. Nicholson[ab]; H. D. Do[a]
[a] School of Engineering, University of Queensland, St Lucia, Qld, Australia [b] Theory and Simulation Group, Department of Chemistry, Imperial College, London, UK

First published on: 21 September 2010

To cite this Article Do, D. D. , Nicholson, D. and Do, H. D.(2009) 'Adsorption in micropores (nanopores): a computer appraisal of the Dubinin equations', Molecular Simulation, 35: 1, 122 — 137, First published on: 21 September 2010 (iFirst)
To link to this Article: DOI: 10.1080/08927020802331349
URL: http://dx.doi.org/10.1080/08927020802331349

Molecular Simulation
Vol. 35, Nos. 1–2, January–February 2009, 122–137

Taylor & Francis
Taylor & Francis Group

Adsorption in micropores (nanopores): a computer appraisal of the Dubinin equations

D.D. Do[a]*, D. Nicholson[ab] and H.D. Do[a]

[a]*School of Engineering, University of Queensland, St Lucia, Qld, Australia;* [b]*Theory and Simulation Group, Department of Chemistry, Imperial College, London, UK*

(*Received 25 March 2008; final version received 25 June 2008*)

Monte Carlo computer simulation in simple pore models was used to investigate the pore filling mechanism proposed by Dubinin for adsorption in activated carbon. The first argument; that adsorption into micropores is primarily due to the potential field exerted by the solid is valid only for small micropores, and the second argument; that molecules fill the space and that the degree of filling depends on the adsorption potential ($RT\ln(p_0/p)$) is partly true. We check the validity of the characteristic curve where isotherms plotted as the logarithm of the density versus the square of the adsorption potential collapse onto a single straight line. We find that linearity is never observed for pores of uniform size, but a single curve is observed, as indicated by the Polanyi theory. For a given characteristic energy, the Dubinin equation corresponds to a solid with a *specific* pore size distribution. Plots of the adsorption heat versus loading follow a complex pattern: initially, they increase or decrease for sufficiently homogeneous or heterogeneous surfaces, respectively; at higher loadings, there is a sharp increase because of the increase of neighbouring molecules and then a sharp decrease because of the increasing importance of repulsion when the adsorbate is very dense.

Keywords: Dubinin equations; adsorption; micropores; isosteric heat

1. Introduction

Since the introduction, in 1947, of the Dubinin–Radushkevich (DR) equation and its many variants afterwards, it has been used extensively to describe the adsorption of vapours in porous carbon [1–6]. The Dubinin equation has the form:

$$\rho_p = \rho_{p,max}\ \exp\left\{-\left(\frac{A}{E}\right)^2\right\}, \tag{1}$$

where ρ_p is the pore density, A is the adsorption potential, $A = \left[RT\ln\left(p_0/p\right)\right]$, p_0 is the vapour pressure and E is the characteristic energy. The DR equation is founded on the Polanyi hypothesis, which states that the amount adsorbed is a function of the adsorption potential (the negative of the difference in free energy between the liquid and adsorbed states). To this Dubinin added the hypothesis that adsorption in micropores proceeded by a volume filling mechanism. Use of the DR isotherm has even been extended to describe adsorption on surfaces [7,8] and adsorption of supercritical fluids [9–12]. The fundamental hypothesis behind this equation is a pore filling mechanism of adsorption, which is brought about because molecules in a pore space are always subject to the potential field exerted by the solid. Deviation of the Dubinin equation from experimental data has been dealt with by using a linear combination of Dubinin equations, either in DR or Dubinin–Astakhov (DA) form [1,2]. Attempts were made by Stoeckli, Jaroniec and Dubinin and co-workers [13–18] to relate the characteristic energy to the structural size of the pore. No matter what form the Dubinin equation takes, the basis behind these variants is pore filling; principally applied to activated carbon with a pore size distribution (PSD). Activated carbon has pores predominantly of approximately slit shape with a range of pore size from about 6 to 30 Å. It is known from numerous molecular simulation studies that, with the exception of very small pores accommodating less than two layers, adsorption in slit pores with graphitic slits follows a layering mechanism, rather than a pore filling mechanism, as postulated by the school of Dubinin. In this paper, we use grand canonical Monte Carlo (GCMC) simulation to investigate argon adsorption at 87.3 K in perfect graphitic pores and in defective pores whose model was proposed recently by Do and Do [19]. The DR equation has been previously studied using simulation by Kaneko and co-workers [20,21], but their study did not bring out the relationship between the characteristic energy with the specific PSD.

2. Theory

In the Monte Carlo simulation, we use the 12-6 Lennard-Jones (LJ) to model the potential energy of interaction between two argon particles, $\varphi = 4\varepsilon\left[\left(\sigma/r\right)^{12} - \left(\sigma/r\right)^{6}\right]$,

*Corresponding author. Email: d.d.do@uq.edu.au

ISSN 0892-7022 print/ISSN 1029-0435 online

DOI: 10.1080/08927020802331349
http://www.informaworld.com

Table 1. Comparison between the simulation results from Gibbs ensemble Monte Carlo (GEMC) and experimental data of vapour pressure, saturated vapour and liquid densities for argon (experimental values are in the brackets).

T (K)	Vapour pressure (kPa)	Saturated vapour density (mol/m^3)	Saturated liquid density (mol/m^3)	Number of particles used in GEMC[a]
77	33.53 (30.9)	53.2 (26.9)	36,419 (41,050)	6000 (155,985)
87.3	100.2 (101.3)	142.4 (146.2)	35,060 (34,848)	1000 (7993)
90	117.6 (133.8)	162.5 (188.4)	34,509 (34,393)	1000 (6994)
100	258 (324.7)	357 (425.2)	32,960 (32,774)	1000 (21,979)
100	277 (324.7)	354 (425.2)	32,935 (32,774)	2000 (29,1971)
120	1048.2 (1213)	1243 (1506)	29,398 (29,009)	1000 (54,946)

[a] The two numbers in the brackets of the last column are the particle numbers in the vapour and liquid boxes, respectively.

where the molecular parameters are $\sigma = 3.405$ nm and $\varepsilon/k_B = 119.8$ K [22]. Here k_B is the Boltzmann constant.

We use GCMC simulation to generate adsorption isotherms of argon at 87.3 K in pores of various sizes in the micropore range. The pore walls are assumed to be either perfect graphitic surface or a defective graphene surface superimposed on graphitic slabs. The perfect adsorbent is modelled as parallel layers of discrete carbon atoms arranged in a hexagonal pattern with carbon–carbon bond length of 1.42 Å [23], while the defective adsorbent is modelled using a recently proposed model by Do and Do [19]. A defective surface is created by starting with a graphitic surface from which a carbon atom is chosen at random. That atom together with its surrounding atoms, lying less than a defect radius R_c from the chosen atom, are then removed. This process is repeated until a given percentage of defects has been achieved. This model of a defective surface is characterised by two parameters, the percentage of defects and the radius of the defect. Although more elaborate models for porous carbons have been investigated recently [24], the simplified geometries studied here are able to capture the salient adsorption behaviour of more complex structures as well as being close to the original proposals of Dubinin and co-workers.

3. Results and discussion

Since the Dubinin equation involves the saturated vapour pressure to calculate the adsorption potential, $A = RT\ln(p_0/p)$, we have to obtain it for the 12-6 LJ potential model used. This is achieved with the Gibbs ensemble Monte Carlo simulation (GEMC). Typically 1000 particles are adequate to obtain reliable results, except when the temperature is low or when the saturated vapour density is very low. For example at 77 K we used 6000 particles. For each Gibbs simulation we ran 50,000 cycles for equilibration and the same number for statistical collection. The results of the simulations are shown in Table 1 with the experimental values shown in the brackets. We used 77, 87.3, 90 and 100 K to test the Dubinin characteristic curve; one of the main features of the Dubinin theory. As seen from this table, the simple 12-6 LJ potential of argon is adequate to describe the bulk properties of vapour–liquid equilibria, especially at 87.3 K. The saturated vapour pressures predicted by the Gibbs ensemble simulation are correlated very well with the Antoine equation, $\ln p_0 = A - B/T$, and this is shown in Figure 1.

The schematic diagram of a defective pore is shown in Figure 2, and Figure 3 shows a typical local density plot for argon adsorption in a 15 Å defective pore with 30% defect and a defect radius of 6 Å. We see clearly that the adsorption proceeds by layering. If the adsorption mechanism followed a pore filling mechanism, the local density plot would be uniform without any clear presence of a peak.

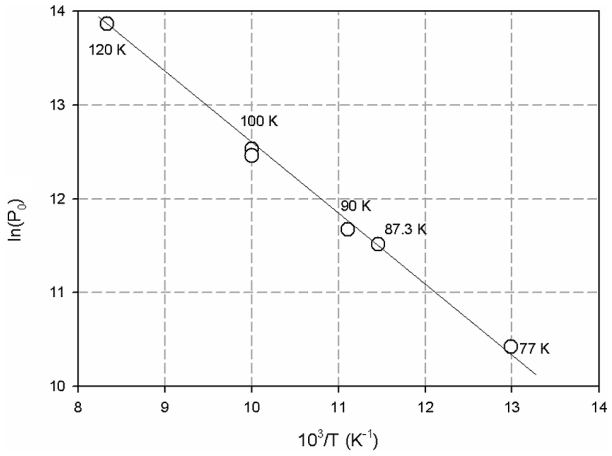

Figure 1. Plot of the logarithm of saturated vapour pressure of argon (from Gibbs simulation) versus the inverse of temperature.

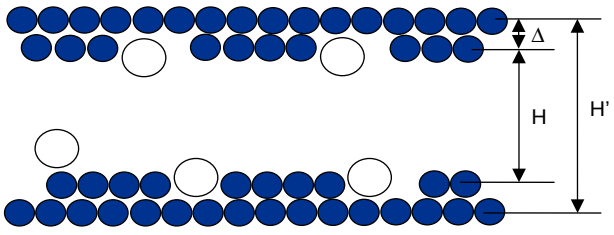

Figure 2. Schematic diagram of a defective pore.

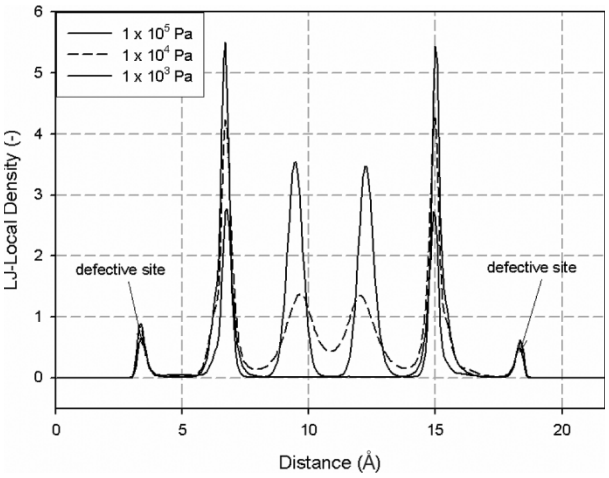

Figure 3. Plot of local density of argon at 87.3 K versus distance from one of the walls in a 15 Å pore whose walls are defective with 30% defect and a defect radius of 6 Å.

Despite the fact that the adsorption follows a layering mechanism, instead of a pore filling one, we tested the validity of the Dubinin equation for a number of slit pores of width: 7, 8, 10, 11.5, 12, 15 and 20 Å. The parameters used in the computer simulation are shown in Table 2. The pore widths chosen include both (near) integer and non-integer multiples of the adsorbate molecular size.

3.1 Adsorption isotherms and DR plots

3.1.1 7 and 8 Å pore

These are ultra-fine pores, according to the Dubinin classification. The adsorption isotherm of argon in the perfect graphitic slit pore is shown in Figure 4 as a solid line with filled symbols.

Since only a single layer can be accommodated in this pore, we do not see any phase transition but rather a smooth increase in density. We support this with a top view of snapshots of argon particles at fractional loadings

Table 2. Parameters used in the GCMC simulation.

Pore size, H (Å)	Reduced pore size $(H - \sigma_{ss})/\sigma$ (dimensionless)	Number of layers	Pore size used in GCMC, H' (Å) (see Figure 2)	Percentage of defect (%)	Defect radius (Å)
7	1.06	1	13.7	0, 30, 50	2.84, 4, 6
8	1.35	Between 1 and 2	14.7		
10	1.94	2	16.7		
11.5	2.38	Between 2 and 3	18.2		
12	2.53	3	18.7		
15	3.41	Between 3 and 4	21.7		
20	4.87	5 layers	26.7		

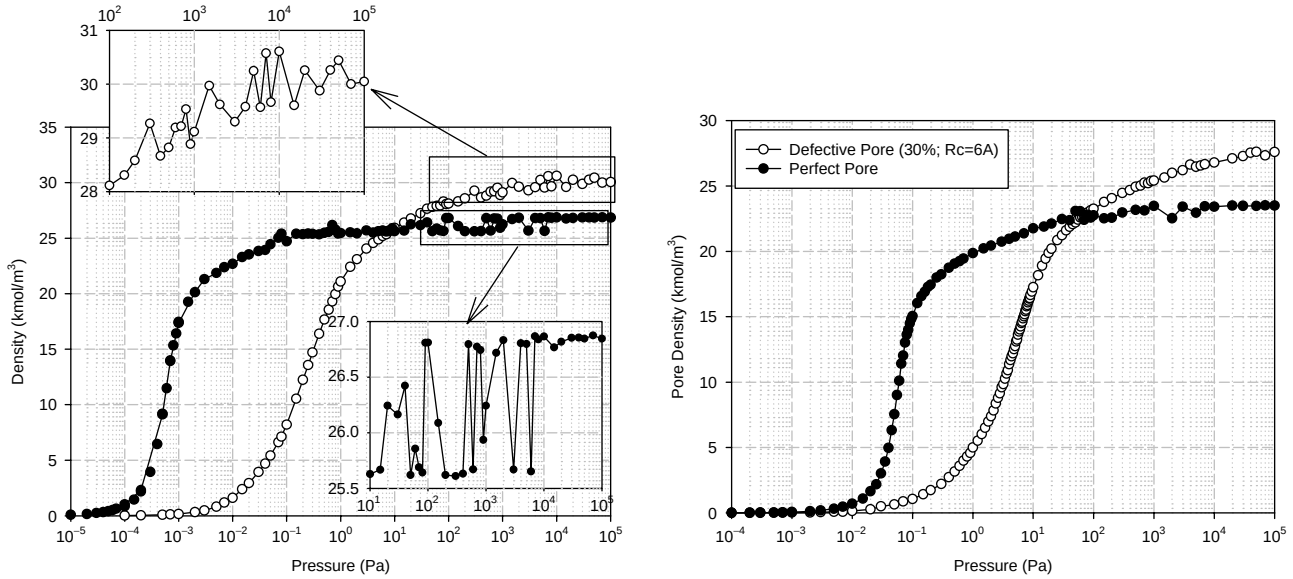

Figure 4. Adsorption isotherms for Ar at 87 K in 7 Å pore (LHS figure) and 8 Å pore (RHS figure). Open symbols for perfect pores while filled symbols for defective pores with 30% defect and a defect radius of 6 Å.

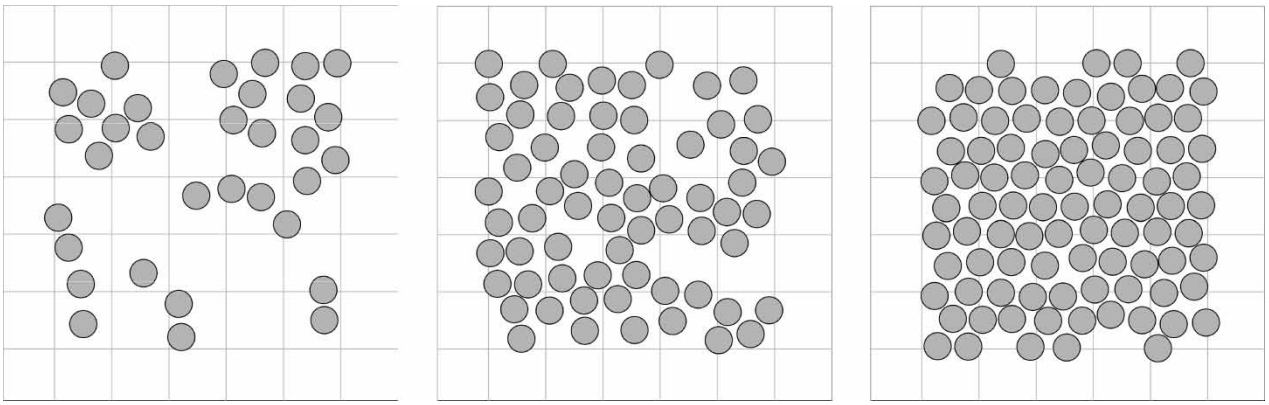

Figure 5. Snapshots of argon particles in perfect 7 Å pore.

of 30, 60 and 100%, respectively, shown in Figure 5. Particles tend to cluster and the size of cluster increases with pressure until they fill the space inside the pore.

The onset of adsorption occurs at very low pressure due to overlapping of the potentials exerted by the two walls. The smooth density variation with pressure appears to support the pore filling mechanism put forward by Dubinin. To test this we plot the results in terms of the Dubinin equation (Equation (1)) by presenting the logarithm of the pore density versus the square of the adsorption potential $A = \left[RT \ln\left(p_0/p\right)\right]$ we should get a straight line whose slope is $-E^{-2}$ and an intercept that is the logarithm of the maximum pore density. Figure 6 (filled symbols) shows a completely different result to the one expected from the DR equation. Instead of a straight line we observe two almost straight lines. This in itself invalidates the use of the Dubinin equation in describing the adsorption in micropores. This conclusion is in agreement with that reached by Kaneko and co-workers [20,21]. If the equation cannot describe adsorption in ultra-fine pores, such as 7 Å pore, it will not describe adsorption in larger pores in the micropore region because these pores also follow adsorption layering, instead of pore filling. Experimentally, two straight lines are often observed from a Dubinin plot; for example for adsorption of carbon dioxide in Linde molecular sieve 4 and 5 Å [1]. Here the two-straight-line behaviour was resolved by combining two Dubinin equations to model the adsorption in two different and independent adsorption volumes. This would imply that each of those volumes that would conform to the Dubinin mechanism.

Clearly the perfect graphitic slit pore does not conform to the Dubinin theory. However, it is pertinent to ask whether pores with rough surfaces might follow the Dubinin equation. We tested this with a slit pore with defective surfaces. With a surface with 30% of defect and a defect radius of 6 Å, we show in Figure 4(a) the adsorption isotherm as the solid line with open symbols. Because of the defects, the onset of adsorption is delayed compared to perfect pores because of weaker affinity, but the variation of pore density with pressure is also smooth, seeming to indicate gradual pore filling. Again, even with

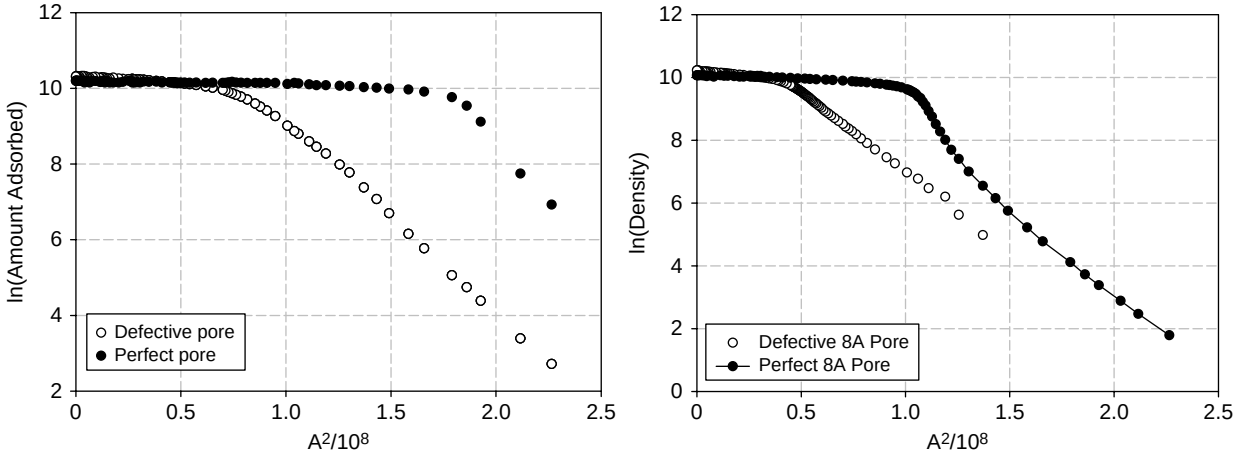

Figure 6. DR plots for Ar at 87.3 K for 7 Å (LHS) and 8 Å (RHS) slit pores with and without defects.

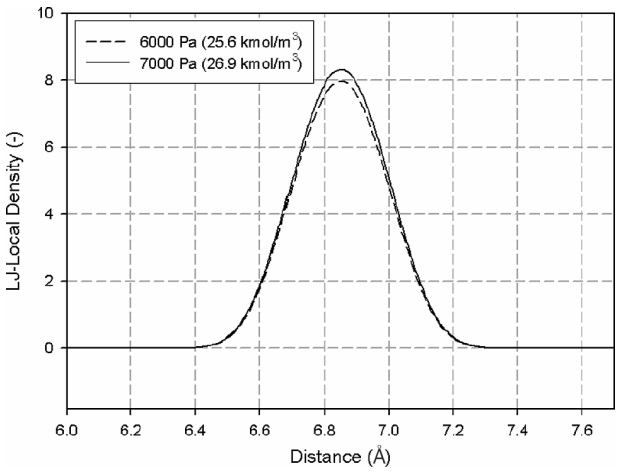

Figure 7. Local density plot of 7 Å pore with perfect walls at two states of high density.

defective surfaces the isotherm does not conform to the DR plot as shown in Figure 6 by open symbols.

For the 8 Å pore, we showed the isotherms for perfect walls and for defective walls in Figure 4(b) and their corresponding DR plots in Figure 6(b). The behaviour is very similar to what we have described for the 7 Å pore, that is: (i) the initial uptake for the perfect pore is greater and (ii) neither pore conforms to the DR plot. Before proceeding to consider larger pores, we particularly note that the isotherm for the 7 Å pore has an interesting behaviour at very high loadings close to saturation. The adsorption capacity then seems to fluctuate between two distinct local states. One state has a capacity of 25.6 kmol/m^3 while the other state has a higher capacity of 26.9 kmol/m^3. This is supported with a local density plot shown in Figure 7. We will discuss the isosteric heat of these two states later in Section 3.2. Packing transitions of methane and CO_2, at saturation in slit shaped pores, have been discussed in terms of Density Functional Theory (DFT) and possible structures [25,26].

So what is left to be explored is whether pores of larger size will conform better to the Dubinin plot. It is not expected that this will be the case, because adsorption in larger pores is expected to have a layering, rather than a pore filling mechanism.

3.1.2 10 Å pore

With perfect walls, this pore can accommodate exactly two integral layers of argon particles. The isotherm for the perfect pore is shown in Figure 8(a) and it exhibits a very sharp transition from gas-like to liquid-like state. Almost immediately after the liquid-like adsorbed phase is formed, it changes to solid-like behaviour. Such sharp transitions from gas–liquid and liquid–solid are due to the very strong adsorption potential exerted by the two opposite walls and the fact that only two layers can be accommodated in this pore. That means that the formation of one layer of one wall enhances the formation of the corresponding layer of the opposite wall. Introducing defects into the two walls destroys this transition as the order is disturbed. This is shown in Figure 8(a) with a defect percentage of 30% and a defect radius of 6 Å. Unlike the ultrafine pore of 7 Å width, adsorption is initiated in the defect as shown in the local density plot versus distance in Figure 8(b) for $P = 1$ and 10 Pa. The fractional loadings at these pressures are less than a few percent. At $P = 1$ Pa, only two peaks at the defect sites are observed, and when pressure is increased to 10 Pa the onset of adsorption of the two interior layers starts. We show in the inset of Figure 8(b) the local density distribution for $P = 100$ kPa, at which we see the dominance of adsorption by the two interior layers, as expected.

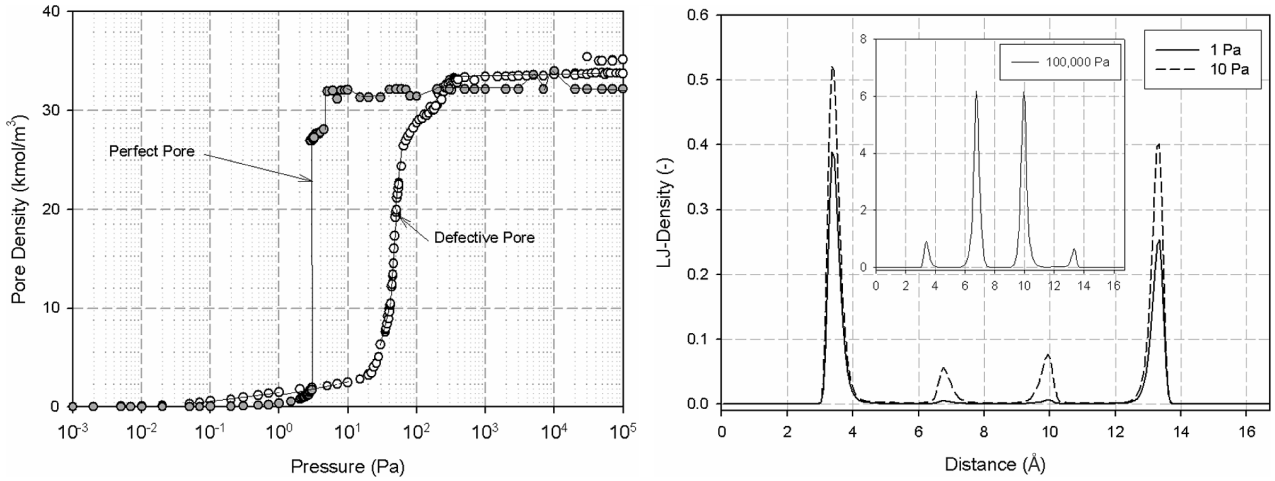

Figure 8. LHS plot, adsorption isotherms of 10 Å pore; RHS, local density plot for 10 Å defective pore.

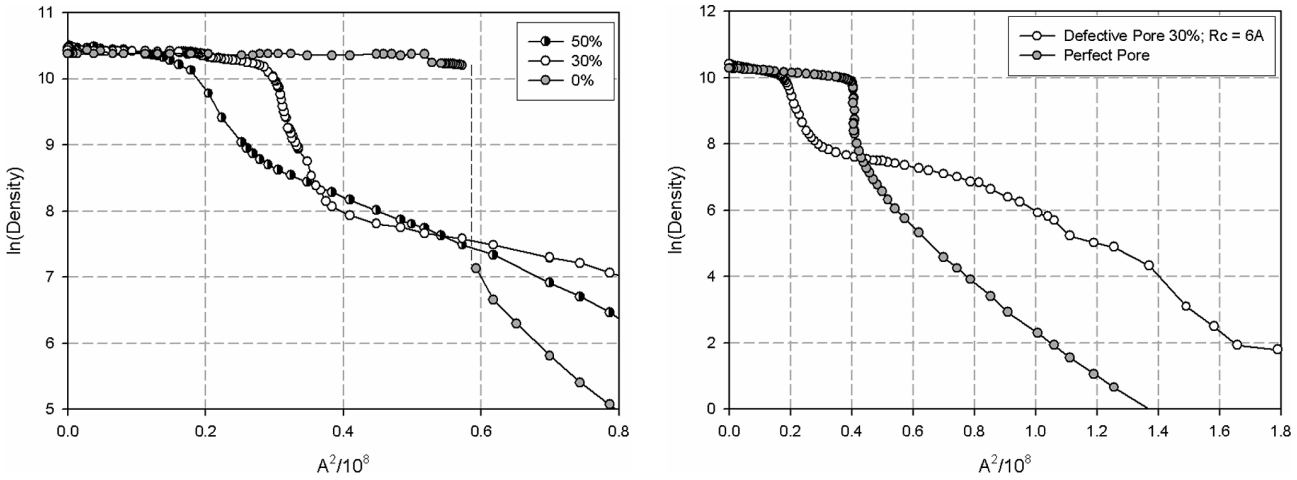

Figure 9. The DR plot of 10 Å pore (LHS) and 11.5 Å (RHS). More than one linear section are observed, and a sharp transition is seen in the perfect pore.

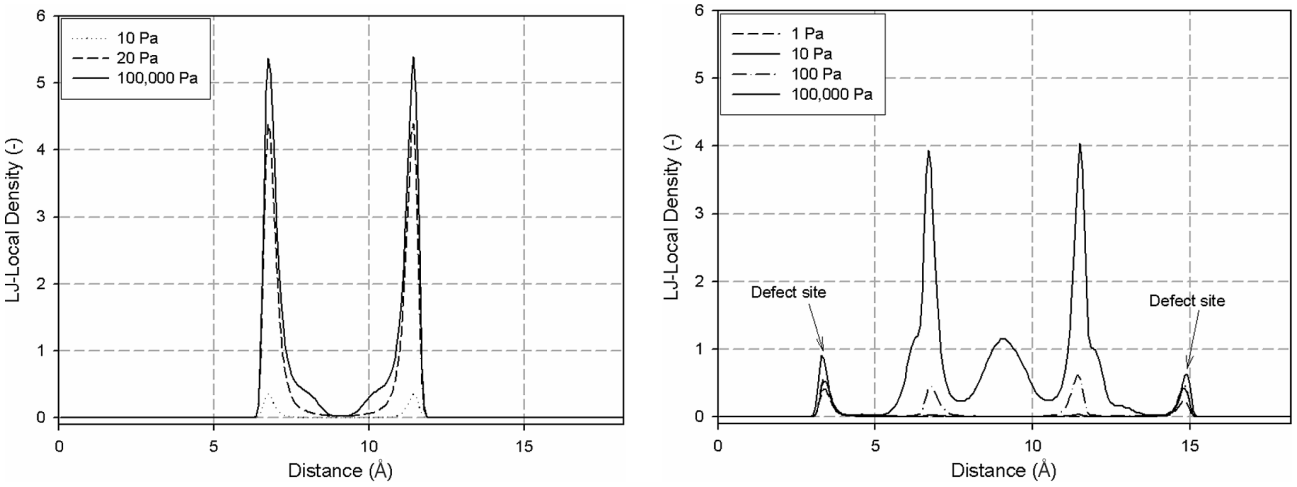

Figure 10. Local density plot for perfect 11.5 Å pore (LHS figure) and defective 11.5 Å pore (RHS figure).

We show in Figure 9(a), the Dubinin plot for the 10 Å pore. Not only do we see two straight lines like those seen for ultra fine pores, but we also observe three linear sections in the DR plot of the logarithm of density versus the square of the adsorption potential. which is in stark contrast to what the DR equation predicts. These examples thus far clearly invalidate the Dubinin equation for the description of adsorption in a microporous solid with a very narrow size distribution. Dubinin and other workers claimed that the DA equation with exponent $n = 3$ instead of 2 in Equation (1) as a better choice for solids with narrow PSD, but we do not see this in our simulation work.

3.1.3 11.5 Å pore

This pore with perfect graphitic walls is too large to accommodate two layers but too small for three layers. Like the other pores that we have dealt with so far, the isotherms of both perfect and defective pores do not conform to the DR plot as seen in Figure 9(b). However, the interesting aspect that arises from the analysis of this

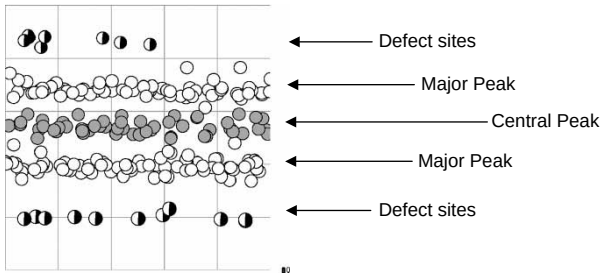

Figure 11. Snapshots of argon particles in defective 11.5 Å pore at 100 kPa.

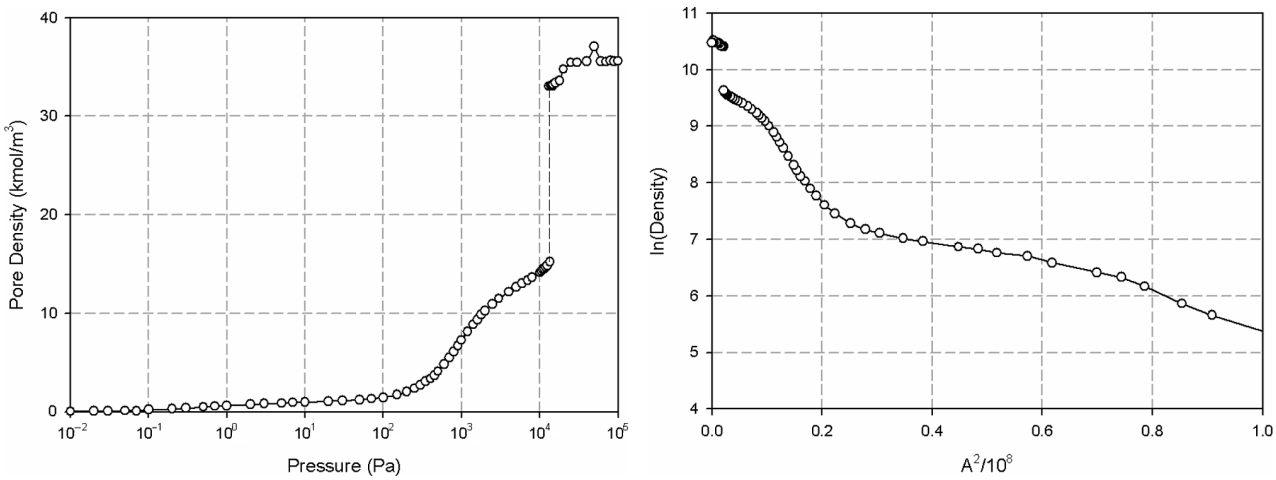

Figure 12. Adsorption isotherm for Ar at 87.3 K, and DR plot for a 20 Å defective pore with 30% defect and a defect radius 6 Å.

pore is when the walls contain defects they can aid in the formation of the third layer in the interior of this pore. In Figure 10(a) are the plots of local density for the perfect 11.5 Å pore. At low pressures we see two distinct peaks, representing two layers. When pressure approaches the saturation pressure, there are two shoulders appearing between the two peaks. These shoulders represent some molecules residing in spaces between the two major peaks, positioned close to the minima of the solid–fluid potential. In the case of the defective pore, adsorption is started from the defect sites as seen with the plots of local density at 1 and 10 Pa. No adsorption in the interior is observed at these pressures. As pressure is increased to 100 Pa, we see the onset of adsorption in the interior. When pressure finally approaches the saturation pressure, we observe a distinct peak for the third layer at the centre of the pore and two shoulders towards the defect sites.

To highlight the inducement of the interior third layer, we present a snapshot of argon particles in Figure 11 for 100 kPa. We use different shading to emphasise particles in different regions. Half filled spheres are argon particles at the defect sites, white spheres are argon at the two major peaks while grey spheres are the third peak at the centre.

3.1.4 20 Å pore

This pore represents the upper limit in the micropore range. For perfect graphitic walls this pore can accommodate five layers of particles. Adsorption is initiated as layering on the two walls and capillary condensation occurs with the complete filling of the three interior layers. The isotherms and the DR plots are shown in Figure 12, and it now comes as no surprise that they do not conform to the DR equation.

We have seen that the Dubinin plot does not apply to uniform pores of any size and any type of surface whether it is a perfect graphitic surface or a defective one. This leads us to consider the hypothesis that a combination of these pores might conform to the Dubinin equation [4–6,15]. By combining the DR plots for pores of various sizes in the same Figure 13, we see that the linear portions for each pore lie in different ranges of the adsorption potential *A*. This suggests that there are combinations of these pores that can give rise to a linear characteristic curve.

The question now is: for a given characteristic energy of the DR equation, what will be the corresponding PSD of an adsorbent that will conform to the DR equation? First, we generate an isotherm from the DR equation (Equation (1)) for a given characteristic energy. The range of the characteristic energy is from 5 to 20 kJ/mol. We then match this DR-generated isotherm against the isotherm

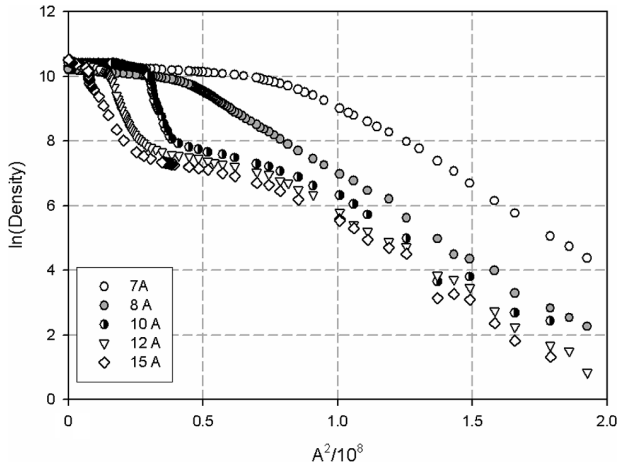

Figure 13. Combined DR plots for defective pores of various sizes.

of a solid having a PSD. The overall adsorption isotherm of this solid is given by:

$$\langle\rho\rangle = \frac{\sum_j V_j\langle\rho\rangle_j}{\sum_j V_j} = \sum_j \alpha_j\langle\rho\rangle_j, \qquad (2)$$

where V_j is the accessible volume of pore having a size H_j. The task is now to optimise the DR equation (Equation (1)) against the overall isotherm calculated from Equation (2) with $\langle\rho\rangle_j$ as the local isotherm of pore j. Results from this

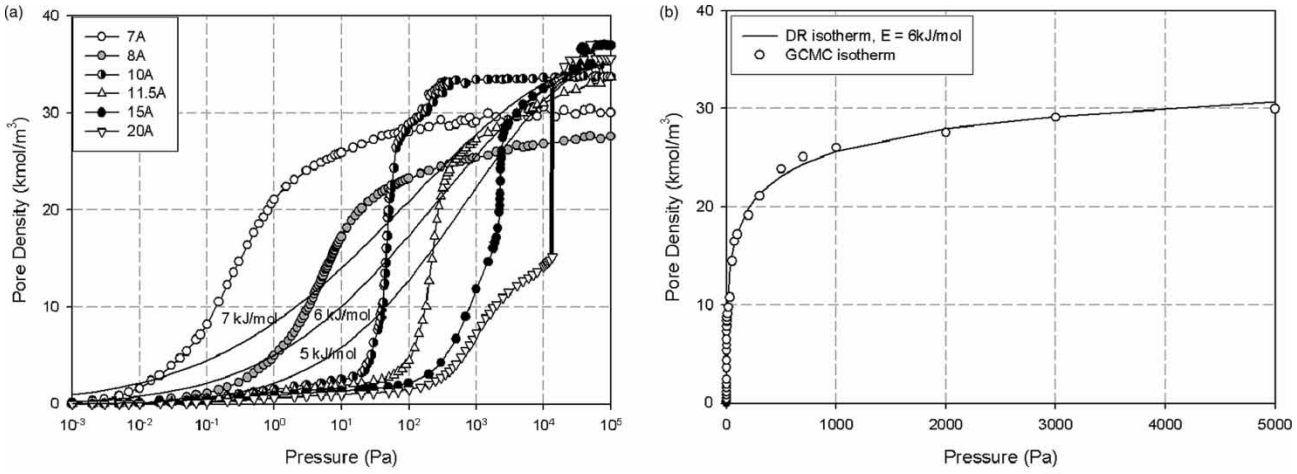

Figure 14. (a) Adsorption isotherms of defective pores of various sizes (symbols) and isotherms calculated with the DR equation (solid lines) for characteristic energies of 5, 6 and 7 kJ/mol; (b) DR isotherm for a solid having $E = 6$ kJ/mol and the computed isotherm using the PSD shown in Figure 15.

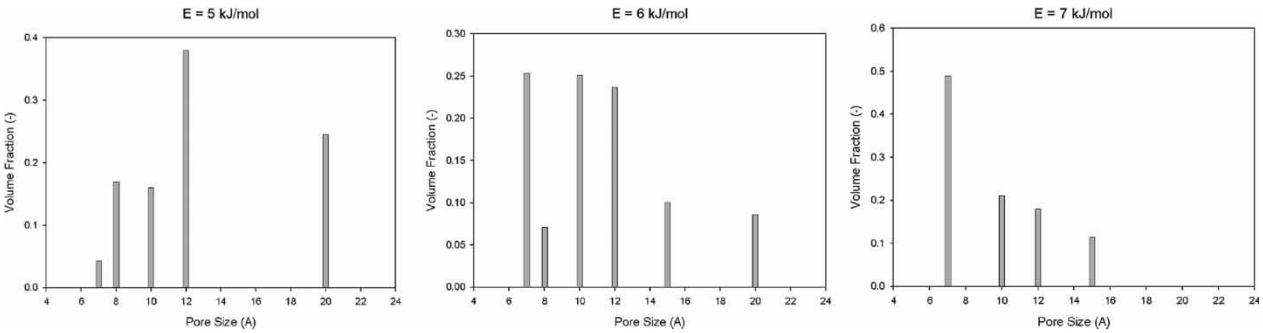

Figure 15. Pore volume distribution derived for different characteristic energy of the DR equation.

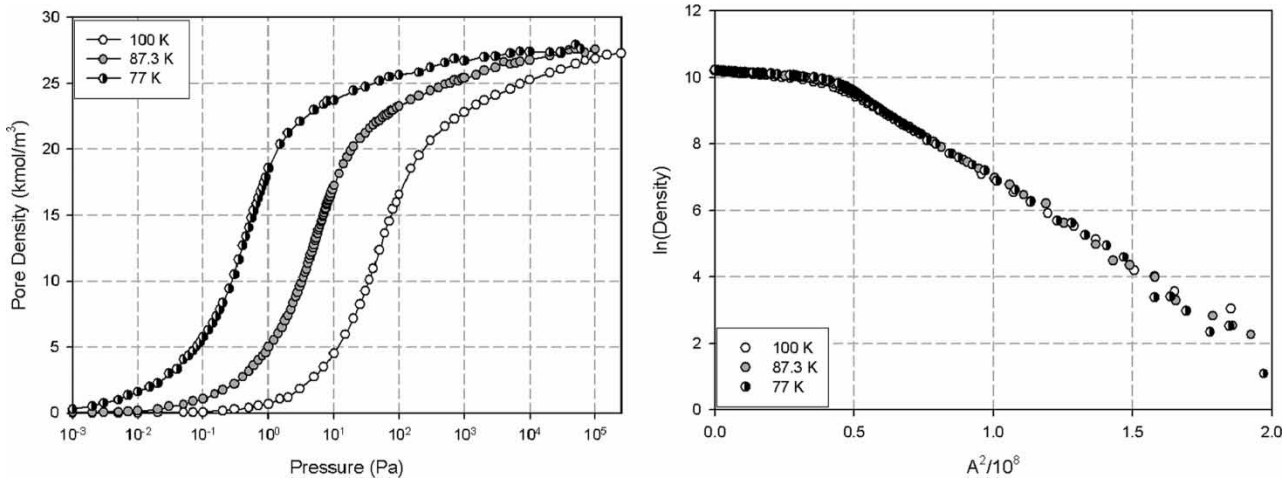

Figure 16. Effects of temperature on the adsorption isotherms of argon in 8 Å defective pore.

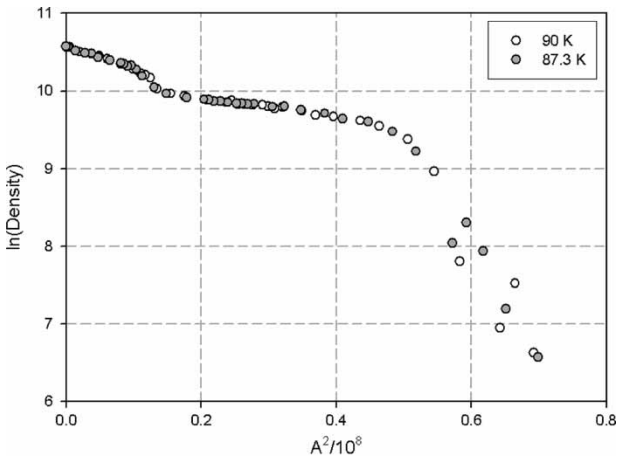

Figure 17. Plot of logarithm of pore density versus the square of the adsorption potential for argon adsorption in cylinder of 10 Å radius at 87.3 and 90 K.

optimisation will yield a set of volume distributions V_j. We have done this with pores having defective graphitic walls. Figure 14(a) shows the adsorption isotherms of argon in defective pores of various sizes at 87.3 K (symbols) as well as isotherms calculated from the DR equation (solid lines) for various values of the characteristic energy. We can see quite clearly that the slopes of the DR-isotherms are quite shallow by comparison with the simulated isotherms, indicating that it is equivalent to the combined results from pores of various sizes. Figure 14(b) shows the good agreement between the DR equation with $E = 6$ kJ/mol and the GCMC simulated isotherm of a porous solid having a specific PSD, and Figure 15 shows the corresponding pore volume distribution for this characteristic energy and for the other choices. It is clear that the DR equation is not valid for an adsorbent with uniform pores, as claimed by the original authors, but rather it is associated with one having a distribution in pore sizes. This also means that each value of the characteristic energy is associated with a PSD, which is in contrast to the claim by many that the characteristic energy is related to one specific pore size ($E = k/x$). Such a relationship is not supported by the computer simulation.

We have established that the DR equation is not applicable to pores of uniform size, but that it does apply to porous solids having a PSD specific for a given characteristic energy. When applied to these solids, the heat pattern is similar to that obtained from GCMC simulation. It is logical then to expect that for these solids the usual DR plot can be applied, as seen in Figure 16(b). This means that the intercept of the DR plot on the ordinate axis does indeed give the correct maximum capacity, but this is strictly true only for solids having a particular PSD! For other distributions this is not correct as we have already shown for pores of uniform size (for example, see Figure 13). Thus we can conclude that the DR equation is applicable only to porous solids with a specific PSD. Figure 15 shows these specific PSDs for three values of characteristic energy, and we particularly note that they are in the range of micropore sizes, typically found in activated carbon. It is therefore not a surprise to find that the DR equations enjoy their applicability to this type of material, but once again we would like to stress that the PSD has to be specific for a given value of characteristic energy. Although the DR equations enjoy widespread use for describing adsorption in activated carbon, it is very often found that they fail to give a linear DR plot. This is usually resolved by using a linear combination of the DR equations, but we can deduce from our investigation that this is merely a correlation exercise, rather than a firm

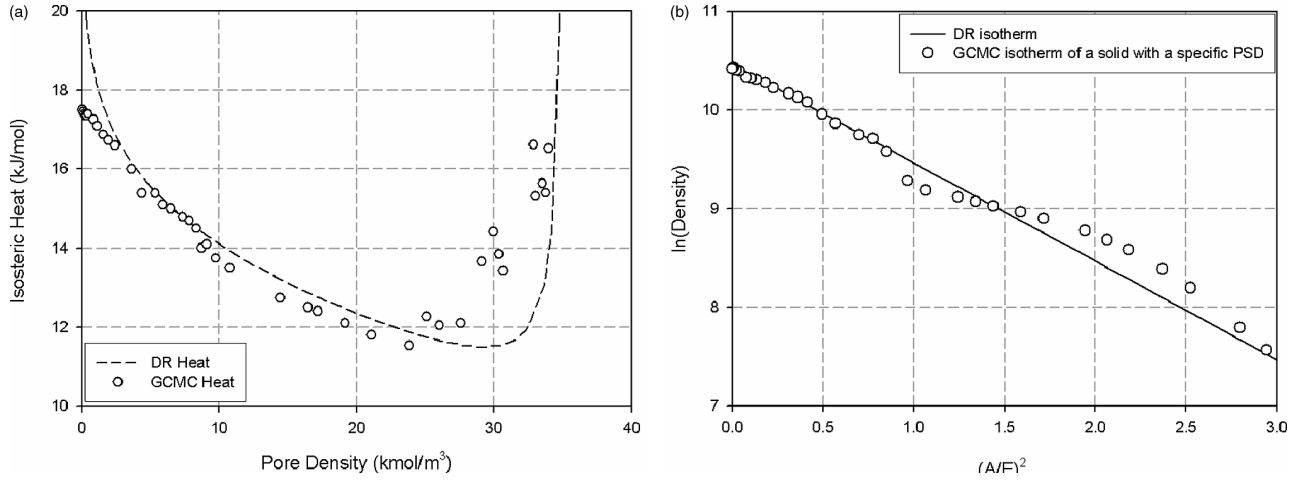

Figure 18. (a) Isosteric heat versus loading obtained from the DR equation (dashed line) and from the GCMC simulation of solid having a specific PSD; (b) the DR plot from the DR equation and from the GCMC simulation.

foundation for choosing such a linear combination of DR equations.

3.1.5 Effects of temperature

We have established that the DR equation is not appropriate for solids with a single pore width but for ones with a PSD. Next, we investigate the temperature effects on the characteristic curve by simulating the adsorption of argon at 77, 87.3 and 100 K on a defective 8 Å pore with 30% defects and a defect radius of 6 Å. The results are shown in Figure 16. Adsorption is greater at lower temperatures, as expected. None of these isotherms conforms to the DR equation. However, they do collapse approximately into one single curve as seen in Figure 16(b). So this aspect of the DR equation, i.e. the temperature invariance of the characteristic curve (the Polanyi hypothesis) is satisfied over a sufficiently narrow temperature range. This was also found to be true for the 10 Å pore, but the results are not shown here.

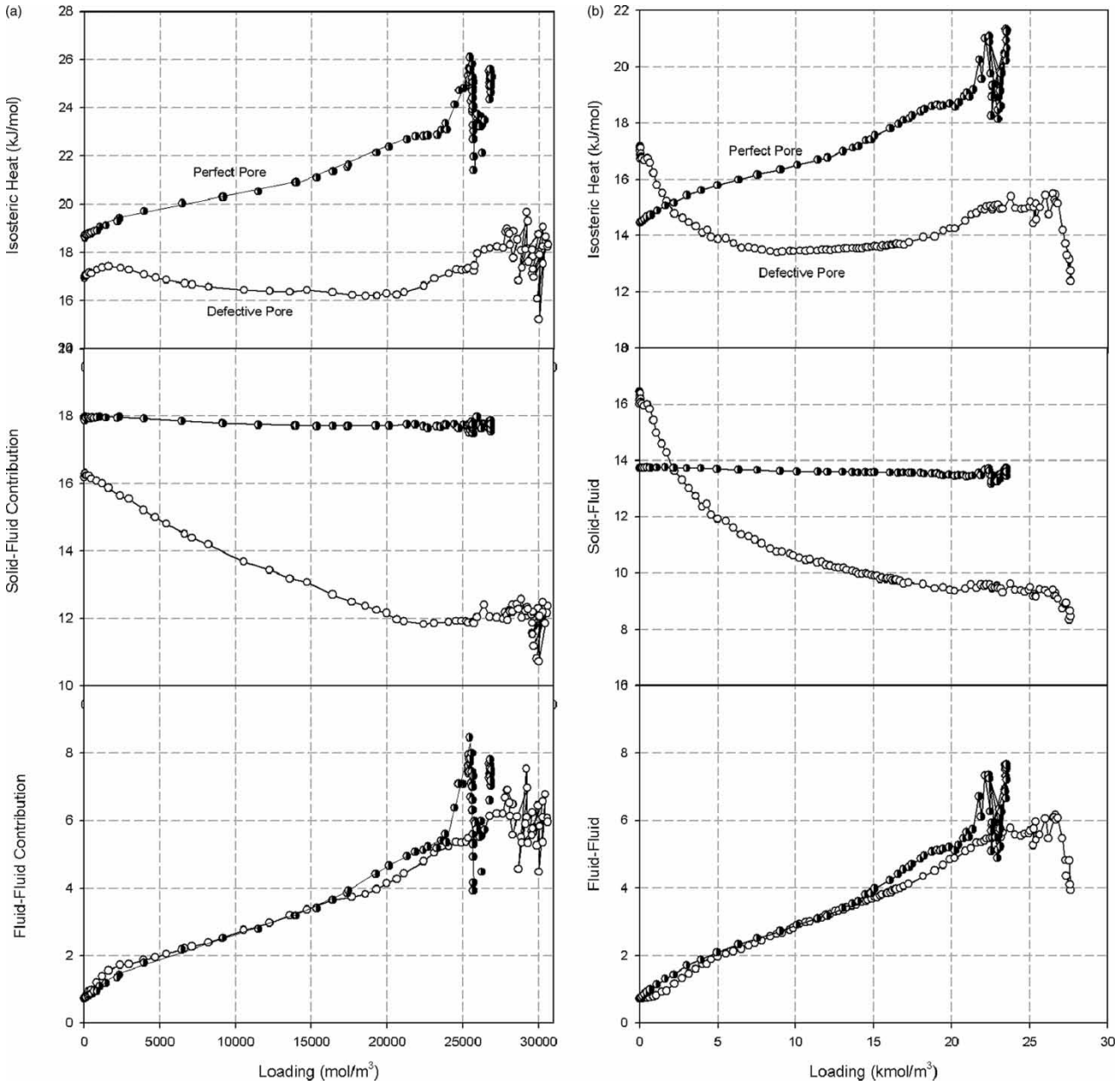

Figure 19. Isosteric heat for Ar at 87.3 K versus loading for: (a) 7 Å pore and (b) 8 Å pore. Half-filled symbols for perfect pores and unfilled symbols for defective pore with 30% defect and a defect radius of 6 Å.

3.1.6 Effects of pore curvature

All the analyses that we have presented thus far are restricted to pores of rectangular geometry. However, a question remains as to whether pores of different geometry could give rise to better agreement with the DR plot. To this end, we use GCMC simulation to generate adsorption isotherms of argon in cylinder of radius 10 Å at 87.3 and 90 K. The simulation results are then presented in the usual Dubinin plot. This is shown in Figure 17, and we do not observe a single straight line in the plot. Once again the use of Dubinin equation proves to be invalid in the description of isotherm for uniform pores. Again however, the single characteristic curve is observed, i.e. two isotherms at different temperatures collapse into one curve when presented in the Polanyi type plot of logarithm of density versus the square of the adsorption potential.

3.2 Isosteric heat

An interesting property that can be obtained from GCMC simulation is the isosteric heat versus loading. This behaves in a complex manner as a function of pore size and of surface characteristics. In this section, we show that a complex pattern of the heat curve versus loading can arise, and this cannot be described by the simple description of heat as predicted by the Dubinin equation. First let us compare the heat obtained from the DR equation with that obtained from the GCMC simulation of porous solids having the specific PSDs as shown in Figure 15.

Given the Dubinin equation with its temperature dependent parameters, we can obtain the isosteric heat by applying the Clausius Clapeyron equation [2]

$$q_{\mathrm{st}} = A + \Delta H_{\mathrm{vap}} + E^2 \delta T / 2A, \tag{3}$$

where A is the adsorption potential, $A = RT \ln(p_0/p)$, ΔH_{vap} is the heat of vaporisation and δ is the temperature coefficient of expansion (of the order of $0.003\,\mathrm{K}^{-1}$ for most liquids). We can now further check the validity of the Dubinin equation by investigating its derived isosteric heat (Equation (3)). This is compared against the heat obtained from the GCMC simulation of a porous solid with a PSD. The required formula for the heat of a porous solid written in terms of the local heats of each pore is [27–29]

$$q_{\mathrm{st}} = \frac{\sum_j \alpha_j \; q_{\mathrm{st},j} \left(\frac{\partial \rho_j}{\partial p}\right)}{\sum_j \alpha_j \left(\frac{\partial \rho_j}{\partial p}\right)}, \tag{4}$$

where $q_{\mathrm{st},j}$ is the local isosteric heat of pore j, which can be calculated from the fluctuation formula [30]:

$$q_{\mathrm{st}} = kT - \frac{\langle UN\rangle - \langle U\rangle\langle N\rangle}{\langle NN\rangle - \langle N\rangle\langle N\rangle}. \tag{5}$$

The gradient of the pore density with respect to pressure can also be obtained directly from the GCMC simulation, as given below:

$$\frac{\partial \rho}{\partial p} = \frac{1}{V} \frac{\langle NN\rangle - \langle N\rangle\langle N\rangle}{kT} \frac{\partial \mu}{\partial p}. \tag{6}$$

For an ideal gas, this equation reduces to:

$$\frac{\partial \rho}{\partial p} = \frac{\langle NN\rangle - \langle N\rangle\langle N\rangle}{pV}. \tag{7}$$

Thus to compute the isosteric heat for a solid at a given pressure p, we obtain the local isosteric heats and the density gradients for all local pores according to Equations (5) and (7). These are then used in Equation (4) to obtain the required results. Figure 16(a) shows the isosteric heat as obtained from the DR equation and from the GCMC simulation. We see that although the heat derived from the

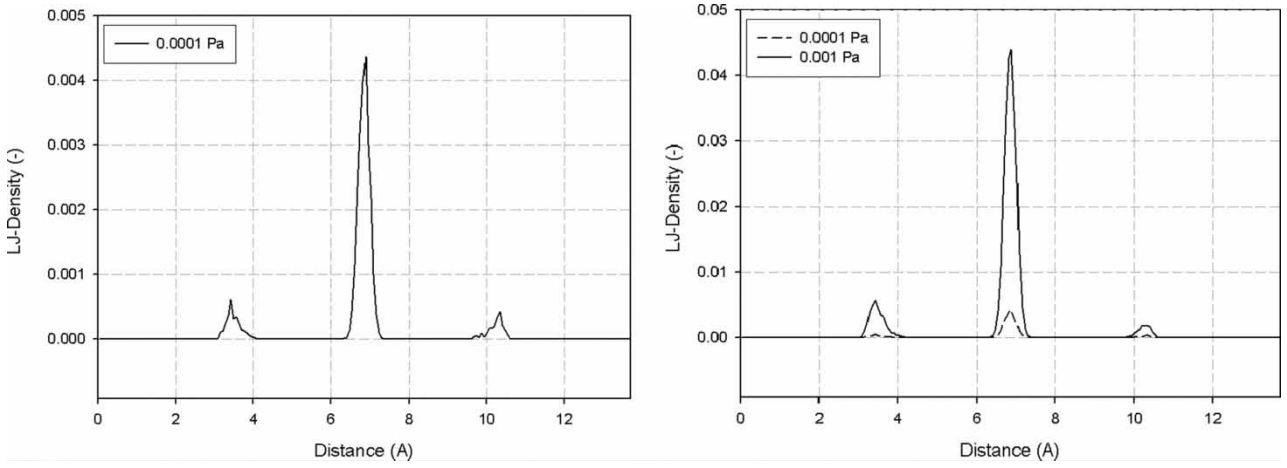

Figure 20. The local density plot for Ar at 87.3 K versus distance for 7 Å defective pore.

DR equation captures the essential pattern obtained from the GCMC simulation, it gives too high a value at very low and very high loadings. The GCMC-derived adsorption isotherm obtained for the solid having a specific PSD follows the usual DR plot (Figure 18(b)), as expected.

3.2.1 Heat patterns in pores of different sizes and defects

It might be expected that at low loadings the isosteric heat of a defective pore will be greater than that of a corresponding perfect pore because defects are strong energy sites because an adsorbate molecule has more adsorbent neighbour atoms. However, this is not found to be the case for very small pores such as 7 Å pore because the degree of overlap of the potentials of the two opposing surfaces is decreased by the presence of defects as discussed earlier. Figure 19(a) shows the isosteric heat versus loading for the 7 Å pores with perfect graphitic walls (filled symbols) and with defective walls (open symbols). The percentage of defects is 30% and the defect radius is 6 Å. The adsorption strength of the pore with perfect walls is greater, and the isosteric heat increases with loading, entirely due to the fluid–fluid interaction. The solid–fluid contribution is practically constant because the adsorbed layer is at the centre of the pore. At very high loadings there are fluctuations in the heat and this is mostly due to the difficulty in the insertion of particles into a very dense adsorbate.

Let us now turn to the defective 7 Å pore. The isosteric heat at zero loading is less than that for a perfect pore, and this is because the initial adsorption actually occurs in the middle of the pore, and since some carbon atoms are missing, the solid–fluid potential is less than that of the corresponding pore with perfect walls. When the loading is increased the heat contributed by the solid–fluid interactions is reduced, due to adsorption onto progressively weaker sites. The heat contributed from the fluid–fluid interactions steadily increases because of the increase in the number of surrounding neighbours. Interestingly the fluid–fluid interaction in a defective pore is practically the same as the corresponding pore with perfect graphitic walls, indicating that interaction among argon particles is similar in this ultra fine pore. To add further support to why adsorption occurs in the centre of the pore in preference to the adsorption at defect sites under dilute conditions, we present in Figure 20 the local density distribution at very low pressure (0.0001 Pa) at which the fraction filling is only 4%. The majority of adsorption is seen in the centre of the pore with very small amount in the defects. At higher pressure (0.001 Pa) at which the fractional filling is 50% we see adsorption is again dominated by the centre of the pore, which is in agreement with the heat contributed by solid–fluid interaction in Figure 19(a) (middle plot).

On moving to larger pores where the overlapping of potentials exerted by the two walls is smaller, we see the greater importance of the strength of the defect sites, i.e. the isosteric heat for a defective pore at zero loading is greater than that for the corresponding perfect pores. This is seen in Figures 19(b) and 21 for 8 and 10 Å pores, where the heat contributed by the solid–fluid interactions is greater in defective pores. A number of features that we can also deduce from these plots are as follows: In small pores (7 and 8 Å) where only one layer can be formed

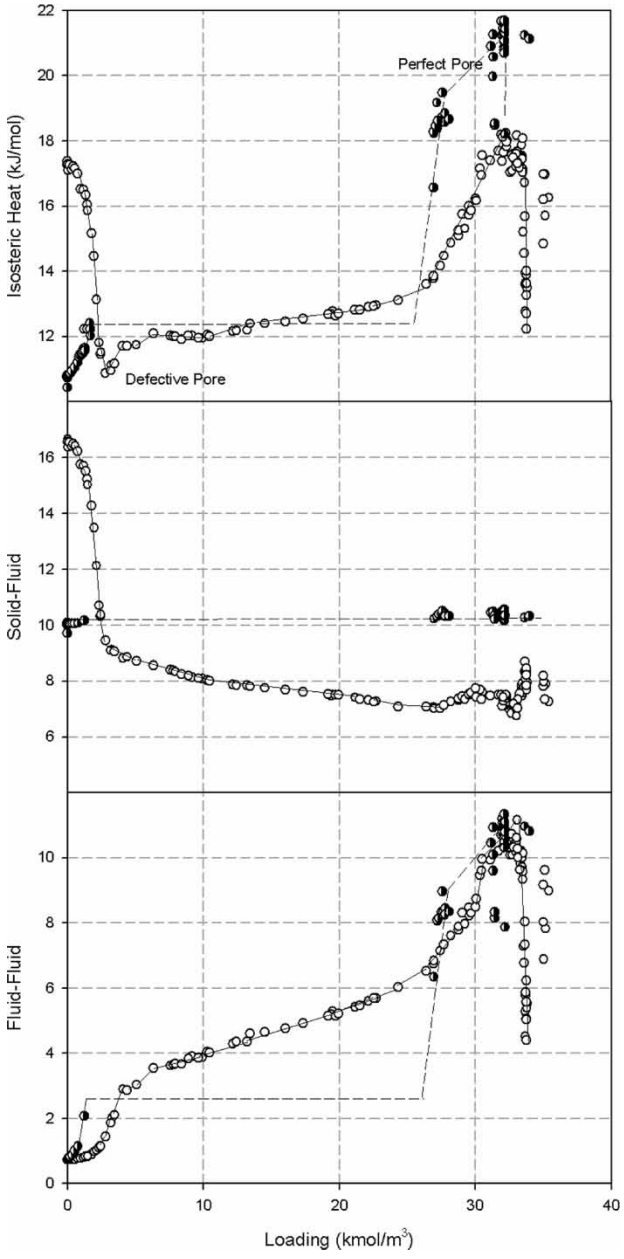

Figure 21. Isosteric heat for Ar at 87.3 K versus loading for 10 Å pore. Half-filled symbols for perfect pores and unfilled symbols for defective pore with 30% defect and a defect radius of 6 Å.

inside the pore (except at the defect sites) the fluid–fluid interaction is the same in both defective and perfect pores. However when considering the 10 Å pore we see the significance of the phase transition which exists in perfect pores. This transition gives rise to the distinct difference in the isosteric heat between the perfect pore and the defective pore. The perfect pore shows a constant heat across the phase transition, indicating the increase in the number of clusters during the transition. The pattern of heat curve for a perfect pore has an initial increase, which is due to the increase of neighbours. The heat is constant across the transition and after the transition the heat further increases, due to the increasing number of neighbours. At very high loadings, the heat decreases and this is due to compression, forcing molecules closer together resulting in a greater contribution from repulsion.

Let us now move to larger pores 12, 15 and 20 Å. The results are shown in Figures 22 and 23. The 12 and 15 Å behave as expected. On the other hand the 20 Å pore

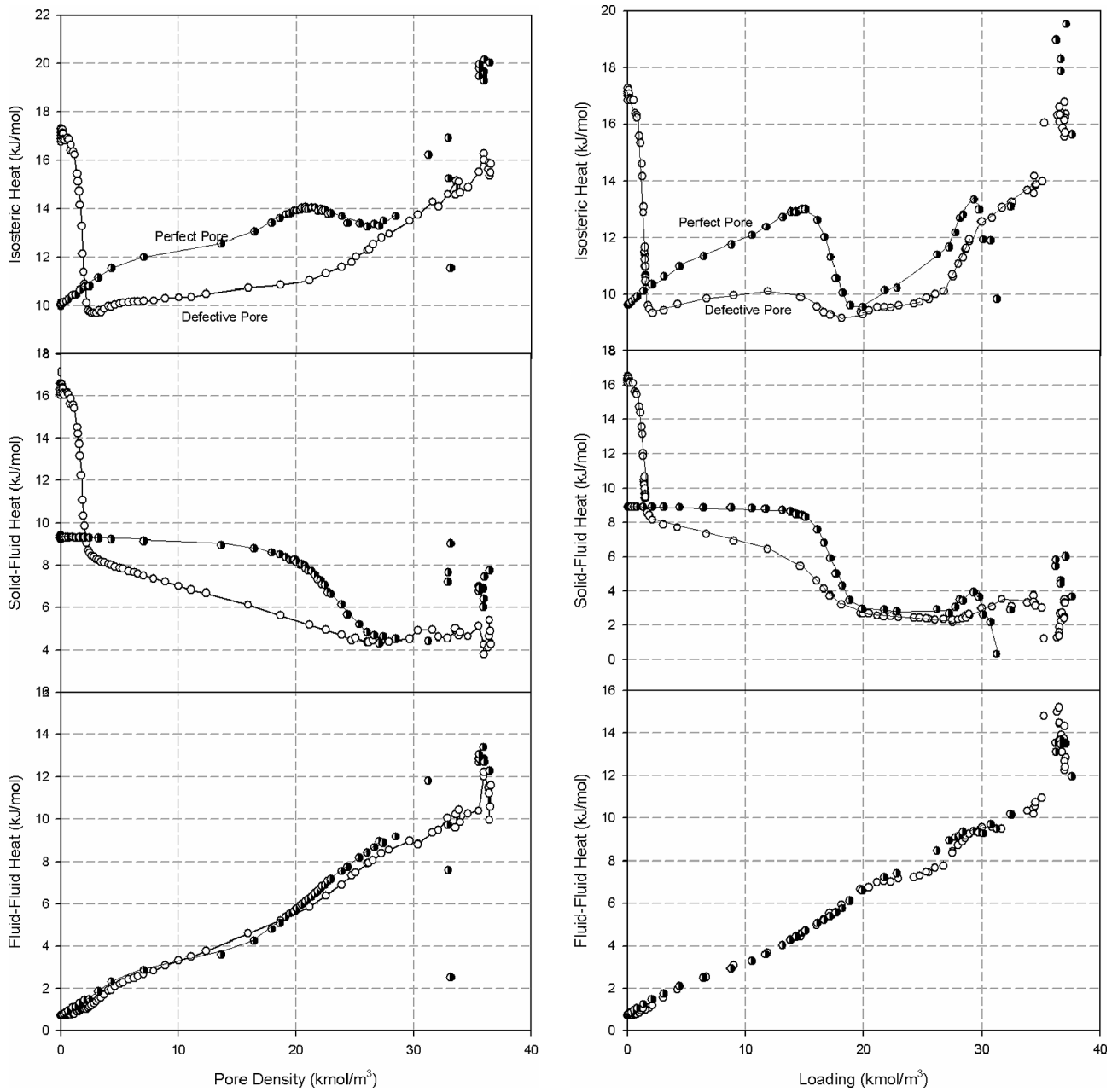

Figure 22. Isosteric heat for Ar at 87.3 K of 12 and 15 Å pores. Half-filled symbols for perfect pores and unfilled symbols for defective pore with 30% defect and a defect radius of 6 Å.

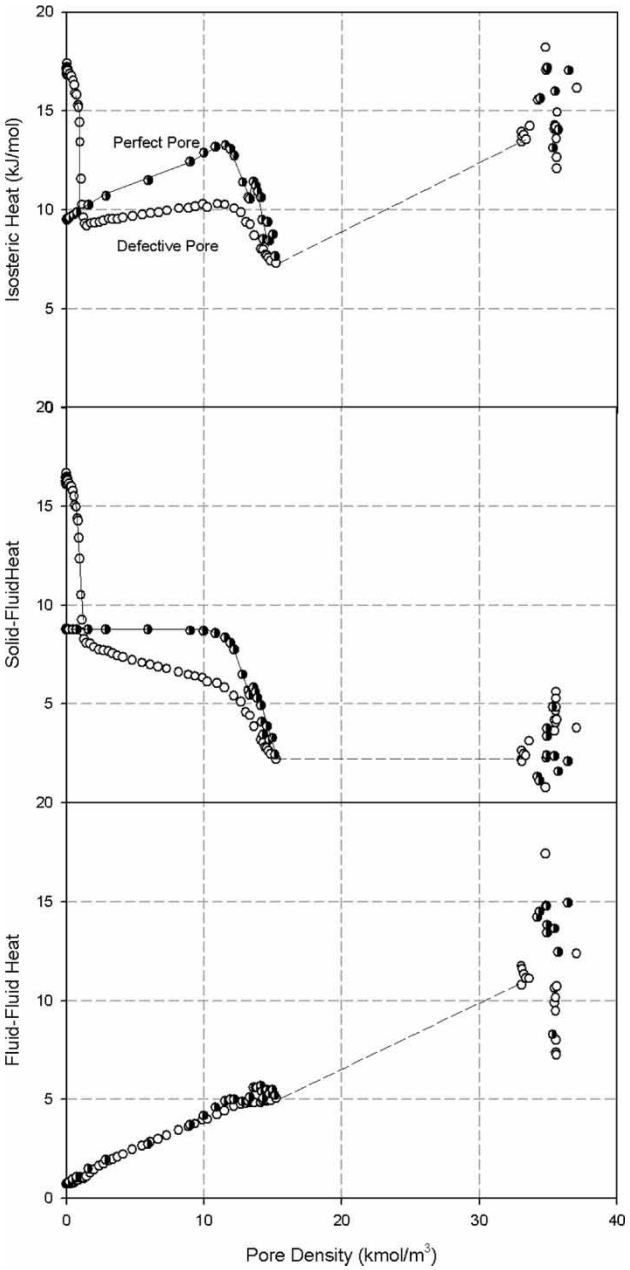

Figure 23. Isosteric heat for Ar at 87.3 K of 20 Å pores. Half-filled symbols for perfect pores and unfilled symbols for defective pore with 30% defect and a defect radius of 6 Å.

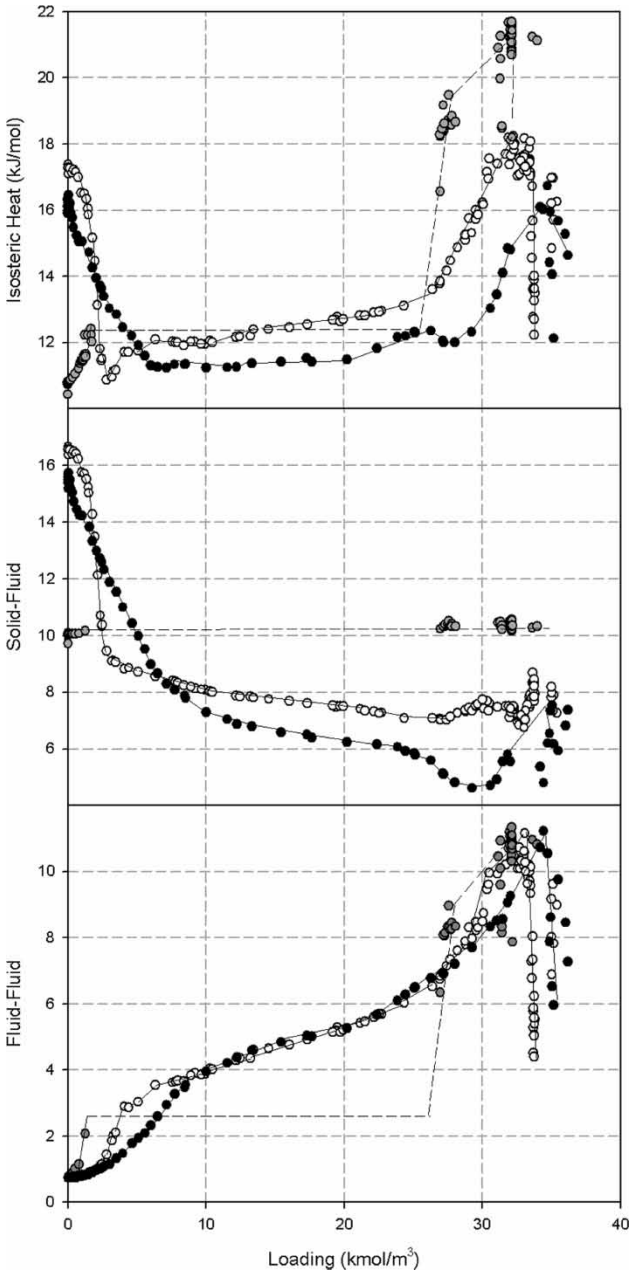

Figure 24. Effects of percentage of defect on the pattern of heat curve. Grey symbols, 0% defect; white symbols, 30% defect; black symbols, 50% defect.

has a capillary condensation and this is reflected in the discontinuity in the isosteric heat versus loading.

3.2.2 *Effects of percentage of defect*

The effects of the percentage of defect are shown in Figure 24 for 10 Å pore. This pore is chosen to show how the extent of defect could destroy the sharp transition in the adsorption isotherm for pores with perfect walls. The pattern of the heat curve changes from a stair-case pattern to a cup holder pattern.

3.2.3 *Effects of the size of defect*

So far we have presented results for defective pores with a defect radius of 6 Å. The size of defect can have an impact on the isotherm as well as isosteric heat. This is seen in Figure 25 for 10 Å with 30% defect and the defect sizes

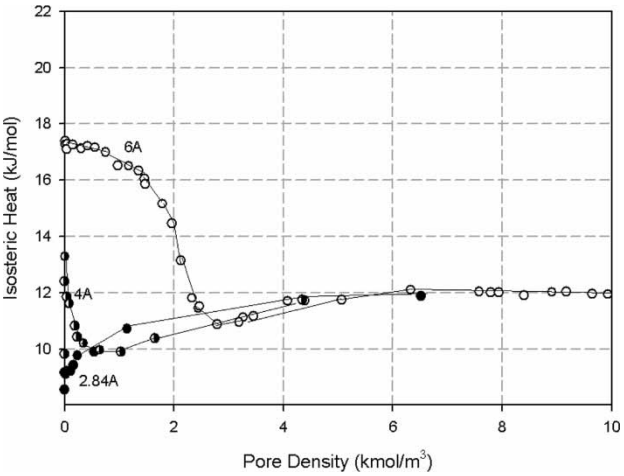

Figure 25. Isosteric heat of defective 10 Å pore. (a) $R_c = 2.84$ Å, (b) $R_c = 4$ Å and (c) $R_c = 6$ Å.

are 2.84, 4 and 6 Å. When the defect size is very small (2.84 Å), we do not see the influence of the site as the pit is too small to create a strong site. As the pit is slightly larger, we start to see some effects and finally when the pit size is 6 Å, we see the significant impact of the defects, influencing the heat curve mainly in the initial stage of adsorption.

3.2.4 Effects of temperature

Finally, we investigate the effects of temperature on the heat curve. We show this for 8 Å pore with 30% of defects and a defect radius of 6 Å in Figure 26. With the exception of a very small but detectable, difference in the isosteric heat at zero loading for higher temperature, we do not see any difference between the two heat curves, suggesting a similar mechanism of adsorption at a given loading.

4. Conclusions

We have presented in this paper, a comprehensive computer simulation of adsorption in pores with either graphitic surface or defective surface, and compared the results with the DR equation. It has been found that the straight line of the DR plot is not observed for pores of any size and of any surface topology. However the characteristic curve conforms to the basis of the DR theory in the sense that isotherms at different temperatures can be collapsed into one curve, satisfying the Polanyi theory. The DR equation is shown to be applicable only to porous solids having a specific PSD, which invalidates the general use of this equation. Finally we discuss the heat curve versus loading as a function of pore size and surface characteristics. The pattern in general can vary from an arm-chair shape to a cup holder shape.

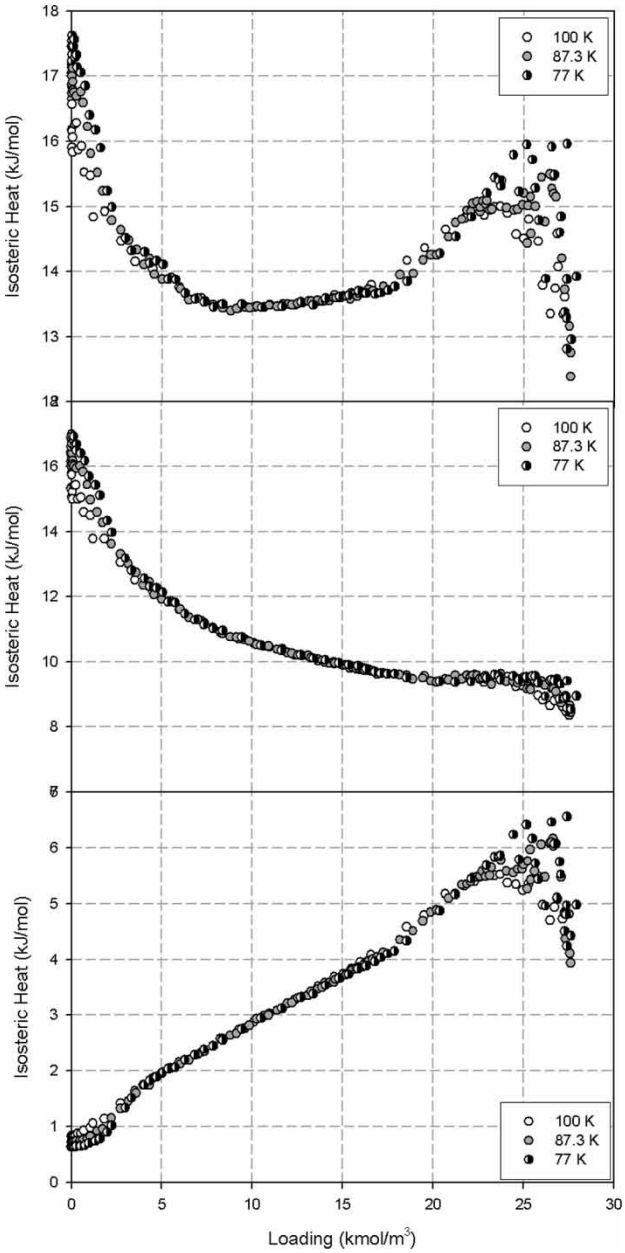

Figure 26. Isosteric heat in defective 8 Å pore at 77, 87.3 and 100 K.

Acknowledgements

Support from the Australian Research Council is appreciated.

References

[1] S.J. Gregg and K.S.W. Sing, *Adsorption, Surface Area and Porosity*, Academic Press, New York, 1982.
[2] D.D. Do, *Adsorption Analysis: Equilibria and Kinetics*, Imperial College Press, London, 1998.

[3] B.P. Bering, V.V. Serpinsky, and M.M. Dubinin, *Thermodynamics of adsorption in micropores*, J. Colloid Interface Sci. 38 (1972), pp. 185–194.
[4] H.F. Stoeckli, *On the theoretical foundation of the Dubinin–Astakhov equation*, Carbon 19 (1981), pp. 325–326.
[5] M. Jaroniec and R. Madey, *Physical Adsorption on Heterogeneous Solids*, Elsevier, Amsterdam, 1988.
[6] W. Rudzinski and D. Everett, *Adsorption of Gases on Heterogeneous Surfaces*, Academic Press, New York, 1992.
[7] M.G. Kaganer, *New method for determining the specific surface of adsorbents and other finely divided substances*, J. Russ. Phys. Chem. 33 (1959), pp. 352–360.
[8] J. Cortes and P. Araya, *The Dubinin–Radushkevich–Kaganer equation*, J. Chem. Soc. Farad. Trans. I 82 (1986), pp. 2473–2479.
[9] S. Ozawa, S. Kusumi, and Y. Ogino, *Physical adsorption of gases at high-pressure 4. Improvement of Dubinin–Astakhov adsorption equation*, J. Colloid Interface Sci. 56 (1976), pp. 83–91.
[10] K.A.G. Amankwah and J.A. Schwartz, *A modified approach for estimating pseudo-vapor pressures in the application of the Dubinin–Astakhov equation*, Carbon 33 (1995), pp. 1313–1319.
[11] M. Aoshima, K. Fukasawa, and K. Kaneko, *Micropore filling of supercritical Xe in micropores of activated carbon fibers*, J. Colloid Interface Sci. 222 (2000), pp. 179–183.
[12] K. Kaneko and K. Murata, *An analytical method of micropore filling of a supercritical gas*, Adsorption 3 (1997), pp. 197–208.
[13] X. Lu, M. Jaroniec, and R. Madey, *Use of adsorption-isotherms of light normal alkanes for characterizing microporous activated carbons*, Langmuir 7 (1991), pp. 173–177.
[14] M.M. Dubinin, *Fundamentals of the theory of adsorption in micropores of carbon adsorbents – characteristics of their adsorption properties and microporous structures*, Carbon 27 (1989), pp. 457–467.
[15] M.M. Dubinin and H.F. Stoeckl, *Homogeneous and heterogeneous micropore structures in carbonaceous adsorbents*, J. Colloid Interface Sci. 75 (1980), pp. 34–42.
[16] M.M. Dubinin, *Adsorption properties and microporous structures of carbonaceous adsorbents*, Carbon 25 (1987), pp. 593–598.
[17] M. Jaroniec and R. Madey, *Physical interpretation of the energy parameter in the Dubinin–Radushkevich equation*, Carbon 26 (1988), pp. 107–108.
[18] M. Jaroniec and R. Madey, *Enthalpy of immersion of a porous solid*, J. Phys. Chem. 92 (1988), pp. 3986–3988.
[19] D.D. Do and H.D. Do, *Modelling of adsorption on nongraphitized carbon surface: GCMC simulation studies and comparison with experimental data*, J. Phys. Chem. B 110 (2006), pp. 17531–17538.
[20] T. Ohba and K. Kaneko, *GCMC study on relationship between DR plot and micropore width distribution of carbon*, Langmuir 17 (2001), pp. 3666–3670.
[21] T. Ohba, T. Suzuki, and K. Kaneko, *Relationship between DR-plot and micropore width distribution from GCMC simulation*, Carbon 38 (2000), pp. 1892–1896.
[22] A. Michels, H. Wijker, and H.K. Wijker, *Isotherms of argon between 0°C and 150°C and pressures up to 2900 atmospheres*, Physica 15 (1949), pp. 627–633.
[23] H. Marsh, *Introduction to Carbon Science*, Butterworth, London, 1989.
[24] T.J. Bandosz, M.J. Biggs, K.E. Gubbins, Y. Hattori, T. Iiyama, K. Kaneko, J. Pikunic, and K.T. Thomson, *Molecular models of porous carbons*, Chem. Phys. Carbon (2003), pp. 41–228.
[25] T.X. Nguyen, S.K. Bhatia, and D. Nicholson, *Close packed transitions in slit shaped pores: Density functional theory study of methane adsorption capacity in carbon*, J. Chem. Phys. 117 (2002), pp. 10827–10836.
[26] S.K. Bhatia, K. Tran, T.X. Nguyen, and D. Nicholson, *High-pressure adsorption capacity and structure of CO_2 in carbon slit pores: Theory and simulation*, Langmuir 20 (2004), pp. 9612–9620.
[27] G.R. Birkett and D.D. Do, *Correct procedures for the calculation of heats of adsorption for heterogeneous adsorbents from molecular simulation*, Langmuir 22 (2006), pp. 9976–9981.
[28] D.D. Do, D. Nicholson, and H.D. Do, *Heat of adsorption and density distribution in slit pores with defective walls: GCMC simulation studies and comparison with experimental data*, Appl. Surf. Sci. 253 (2007), pp. 5580–5586.
[29] D.D. Do and H.D. Do, *Isotherm and heat of adsorption in porous solids with defective pores-adsorption of argon and nitrogen at 77 K in Saran activated carbon*, Mol. Sim. 33 (2007), pp. 821–837.
[30] D. Nicholson and N. Parsonage, *Computer Simulation and The Statistical Mechanics of Adsorption*, Academic Press, London, 1982.